Appendix 1

DNA extraction and library construction

Sample processing, genomic DNA extraction, library construction, and targeted next-generation sequencing (NGS) were performed in a clinical testing laboratory certified by Clinical Laboratory Improvement Amendments (CLIA) and accredited by the College of American Pathologists (CAP) (36,37). In brief, FFPE samples of the primary tumor were first de-paraffinized with xylene, followed by extraction of genomic DNA using QIAamp DNA FFPE Tissue Kit (Qiagen, No. 56404) according to the manufacturer's instructions. Peripheral blood was centrifuged at 1800g for 10 min, followed by cell-free DNA extraction and purification using QIAamp Circulating Nucleic Acid Kit (Qiagen, No. 55114). As a normal control, the genomic DNA of white blood cells in sediments was also extracted using the DNeasy Blood and Tissue Kit (Qiagen Cat. No. 69504). Nanodrop2000 (Thermo Fisher Scientific, Waltham, MA) was used to assess DNA quality, and Bioanalyzer 2100 (Agilent Technologies) was used to analyze DNA fragment distribution. DNA quantification was performed using the dsDNA HS assay kit on a Qubit 3.0 fluorometer (Life Technology, US).

Hybridization-based target enrichment was carried out using the PULMOCAN™ panel (Nanjing Geneseeq Technology Inc., Nanjing, China) targeting 139 lung cancer-relevant genes (38,39). The hybridization capture reaction was performed using Dynabeads M-279 (Life Technologies, San Diego, CA) and xGen Lockdown hybridization and wash kit (Integrated DNA Technologies) according to the manufacturer's instructions. Captured libraries were then amplified using the KAPA HiFi HotStart ReadyMix (KAPA Biosystems) and purified using Agencourt AMPure XP beads. Libraries were sequenced on the Illumina HiSeq4000 platform according to the manufacturer's instructions.

Data processing and mutation calling

Sequencing reads were demultiplexed and those with low quality and extra N bases were removed using Trimmomatic [5]. Filtered data that passed quality control were then mapped to the human reference genome hg19 using Burrows-Wheeler Aligner (BWA-mem, v0.7.12; https://github.com/lh3/bwa/tree/master/bwakit). The Genome Analysis Toolkit (GATK 3.4.0; https://software.broadinstitute.org/gatk/) was used for local realignment and recalibration of the base quality score. Picard was used to remove duplicates. VarScan2 (40) was used to detect single-nucleotide variations (SNVs) as well as insertion/deletion (Indel) mutations. SNVs were filtered out if the variant allele frequency (VAF) was less than 1%. Additionally, we excluded SNVs that were present in >1% population in the 1000 Genomes Project or the Exome Aggregation Consortium 65,000 exomes database. The resulting mutation list was then compared to an in-house list based on a normal pool of whole blood samples to remove recurrent artifacts. Parallel sequencing of matched white blood cells was performed to remove sequencing artifacts, germline variants, and clonal hematopoiesis. Copy number variant (CNV) analysis was performed using FACETS as previously described (41). Copy-number gain and loss were defined as normalized gene ratio ≥2 or ≤0.6, respectively. Structural variants were identified by FACTERA with default parameters (≥ 2 reads) (42). Fusion reads were manually reviewed and confirmed on Integrative Genomics Viewer (IGV). Variant calling was validated with CLIA/CAP accreditation.

References

36. Yang Z, Yang N, Ou Q, et al. Investigating Novel Resistance Mechanisms to Third-Generation EGFR Tyrosine Kinase Inhibitor Osimertinib in Non-Small Cell Lung Cancer Patients. Clin Cancer Res 2018;24:3097-107.
37. Shu Y, Wu X, Tong X, et al. Circulating Tumor DNA Mutation Profiling by Targeted Next Generation Sequencing Provides Guidance for Personalized Treatments in Multiple Cancer Types. Sci Rep 2017;7:583.
38. Zhang C, Zhang J, Xu FP, et al. Genomic Landscape and Immune Microenvironment Features of Preinvasive and Early Invasive Lung Adenocarcinoma. J Thorac Oncol 2019;14:1912-23.
39. Zhao W, Song A, Xu Y, et al. Rare mutation-dominant compound EGFR-positive NSCLC is associated with enriched kinase domain-resided variants of uncertain significance and poor clinical outcomes. BMC Med 2023;21:73.
40. Bolger AM, Lohse M, Usadel B. Trimmomatic: a flexible trimmer for Illumina sequence data. Bioinformatics 2014;30:2114-20.

https://dx.doi.org/10.21037/tlcr-2025-545

41. Koboldt DC, Zhang Q, Larson DE, et al. VarScan 2: somatic mutation and copy number alteration discovery in cancer by exome sequencing. Genome Res 2012;22:568-76.
42. Riaz N, Havel JJ, Makarov V, et al. Tumor and Microenvironment Evolution during Immunotherapy with Nivolumab. Cell 2017;171:934-949.e16.
43. Newman AM, Bratman SV, Stehr H, et al. FACTERA: a practical method for the discovery of genomic rearrangements at breakpoint resolution. Bioinformatics 2014;30:3390-3.

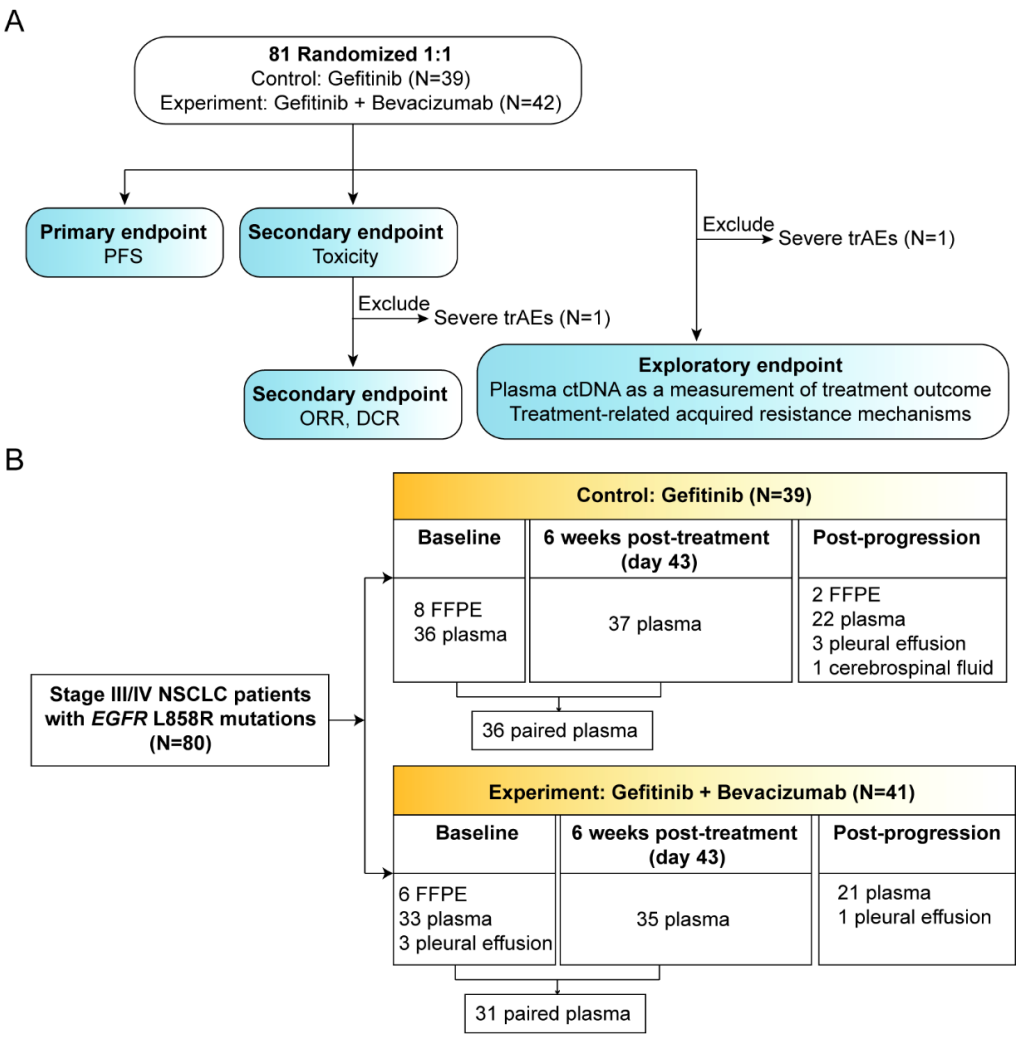

Figure S1 Overview of the trial design and patient samples. (A) A total of 81 patients with *EGFR* exon 21 L858R mutations were randomized at a ratio of 1:1 into the control population where 39 patients were treated with the EGFR tyrosine kinase inhibitor gefitinib, and the experimental population where 42 patients received gefitinib plus bevacizumab combination therapy. One patient experienced severe treatment-related adverse events (trAEs) while receiving the combination therapy, leading to an adjustment of the treatment regimen. Subsequent analyses for treatment response and exploratory endpoints were conducted on a cohort of 80 patients. (B) Clinical samples, including formalin-fixed paraffin-embedded (FFPE) tumor, plasma, pleura effusion, and cerebrospinal fluid, were collected for genomic testing through targeted next-generation sequencing.

https://dx.doi.org/10.21037/tlcr-2025-545

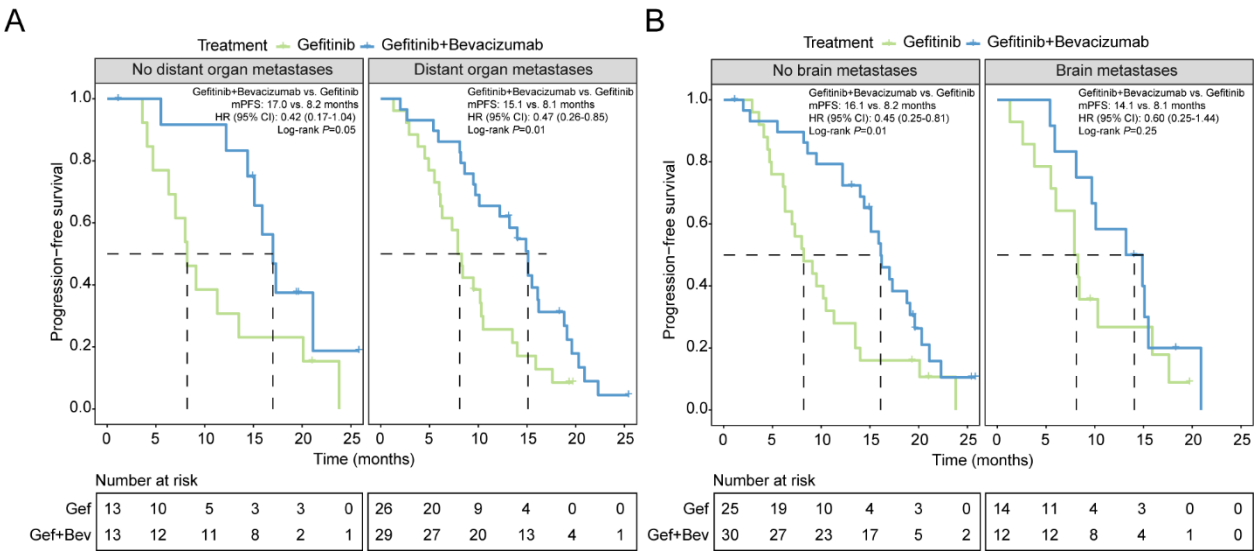

Figure S2 Efficacy of gefitinib plus bevacizumab versus gefitinib monotherapy in *EGFR* L858R-mutated NSCLC patients categorized based on metastatic status. Kaplan-Meier curves of the progression-free survival in patients receiving monotherapy or combination therapy stratified by distant organ metastases (A) and brain metastases (B).

https://dx.doi.org/10.21037/tlcr-2025-545

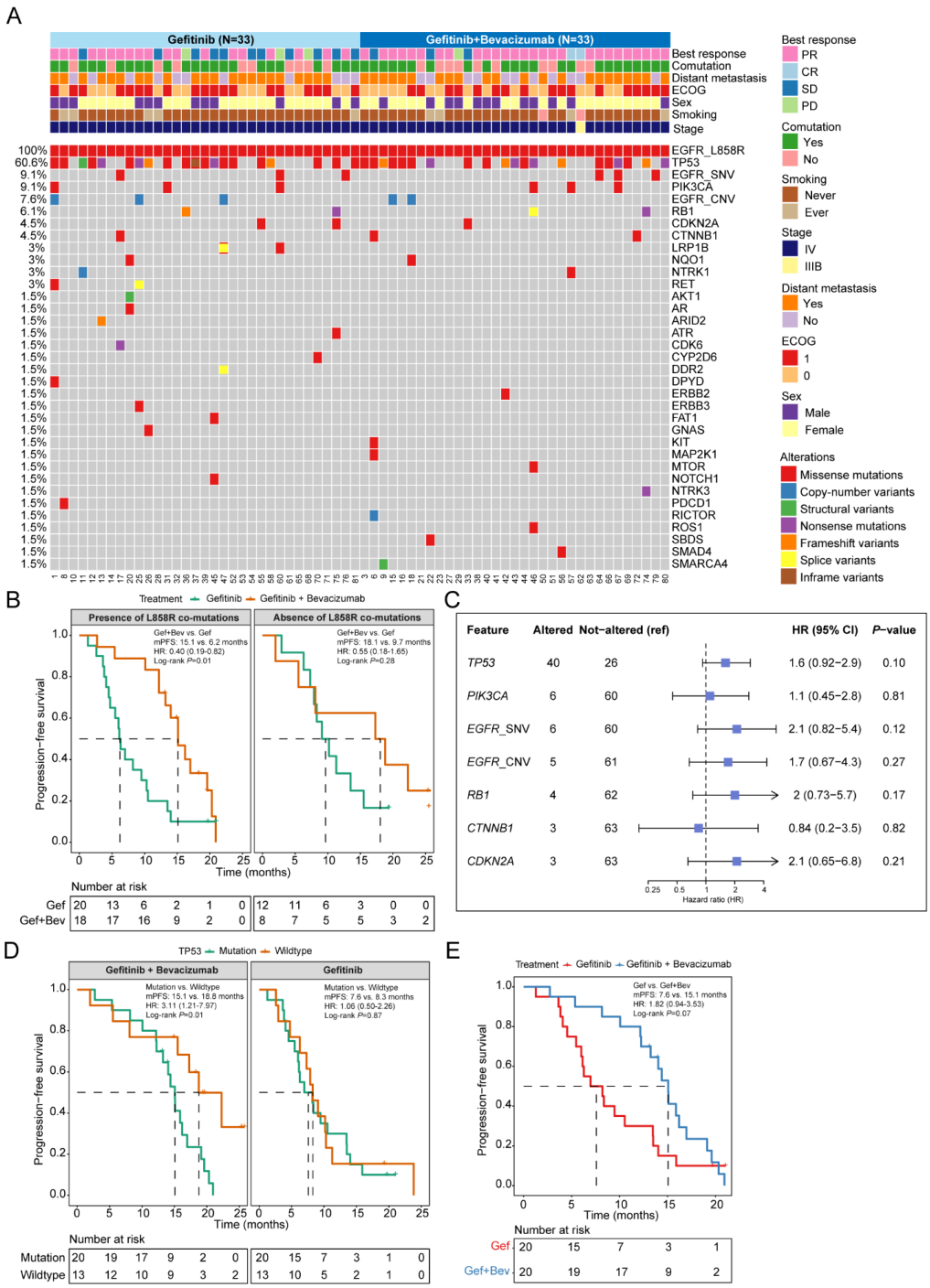

Figure S3 Mutational landscape of baseline *EGFR* L858R-mutated NSCLC patients. (A) Patients with detectable somatic variants in baseline samples were categorized based on treatment. Each column represents one patient, and the mutational frequency of each gene was shown on the left. (B) Kaplan-Meier curves of the progression-free survival (PFS) in patients treated with gefitinib only and in those treated with gefitinib plus bevacizumab after subgrouping based on whether present with L858R co-mutations. (C) The univariate analysis of PFS for genomic alterations with a mutational count ≥3 in baseline samples. (D) Kaplan-Meier curves of the PFS in *TP53*-mutated versus *TP53*-wildtype patients in the combination and monotherapy treatment groups. (E) Kaplan-Meier curves of the PFS in *TP53*-mutated patients treated with combination therapy versus monotherapy.

https://dx.doi.org/10.21037/tlcr-2025-545

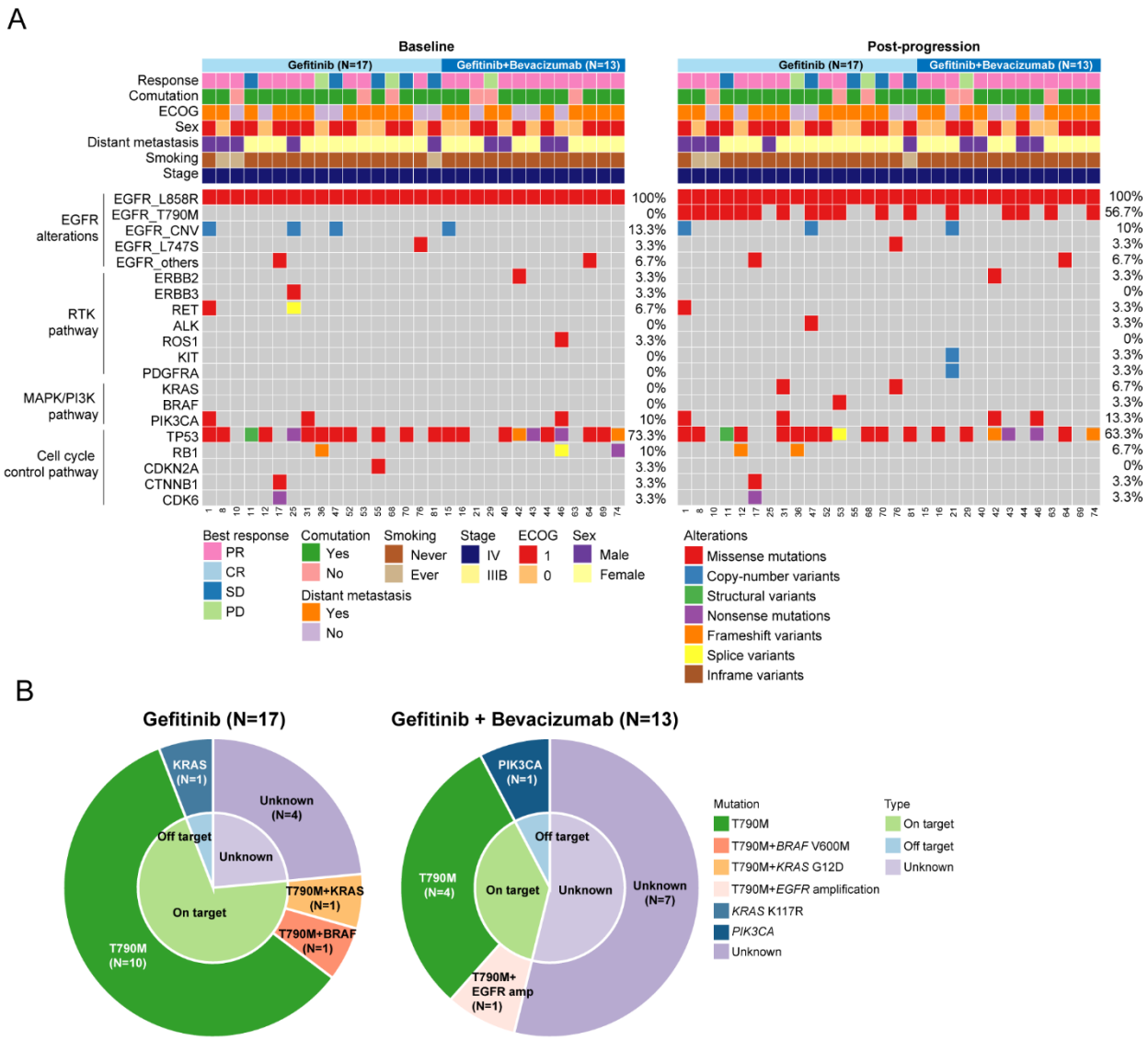

Figure S4 Exploring the underlying acquired resistance mechanism in post-progression patients. (A) Heatmap shows the molecular profile of each patient at baseline (left) and post-progression (right). Patients were clustered based on the type of treatment received. (B) Acquired resistance mechanism in post-regression patients categorized based on treatment.

https://dx.doi.org/10.21037/tlcr-2025-545